Mathematical modelling of thermal runaway in semiconductor laser operation

EINDHOVEN UNIVERSITY OF TECHNOLOGY
Department of Mathematics and Computing Science

RANA 00-12
May 2000

Mathematical modelling of thermal runaway in semiconductor laser operation

by

W.R. Smith

Reports on Applied and Numerical Analysis
Department of Mathematics and Computing Science
Eindhoven University of Technology
P.O. Box 513
5600 MB Eindhoven, The Netherlands
ISSN: 0926-4507

Mathematical modelling of thermal runaway in semiconductor laser operation

W. R. Smith

Department of Mathematics and Computing Science, Technische Universiteit Eindhoven, PO Box 513, 5600 MB Eindhoven, The Netherlands

A mathematical model describing the coupling of electrical, optical and thermal effects in semiconductor lasers is introduced. Through a systematic asymptotic expansion, the governing system of differential equations are reduced to a single second-order boundary value problem. This highly nonlinear equation describes the time-independent maximum temperature in the boundary layer adjacent to the mirror facet. The solution of the problem is a multi-valued function of current. The graph of the maximum steady-state temperature as a function of current gives a fold-shaped response curve, which indicates that no bounded steady state exists beyond a critical value of current. For certain device parameters and initial conditions, thermal runaway occurs. A mechanism for the sudden mode of semiconductor laser failure is described in terms of thermal runaway.

I. INTRODUCTION

The basic property of thermal runaway is that the temperature blows up at some point in the domain at a finite time for the appropriate choices of parameters and initial conditions. The most celebrated example of thermal runaway occurs in combustion theory (see [1] and references therein). The physical reason for this is the positive feedback associated with the exponential source term, which occurs in the large activation-energy limit of the Arrhenius law of chemical kinetics. The use of microwaves to sinter or join ceramics is another application of thermal runaway (see [2]). In the case of ceramics, the positive feedback in the nonlinear source term is in the model for the effective conductivity. Other examples include autocatalytic chemical reactions and electrical heating (see [3] and references therein). In this paper, the failure mechanisms for semiconductor lasers will be studied in terms of thermal runaway. The physical process providing the positive feedback here will be the highly nonlinear temperature dependence of the photon absorption.

A schematic cross-section of a typical semiconductor laser is shown in Figure 1. Semiconductor lasers have been developed for many applications, for example, optical fibre transmission systems. However, these devices suffer from new types of degradation and failure mechanisms. These degradation modes have been split into three categories, based on the rate of change of the device characteristics, namely rapid, gradual and sudden (see [4] and references therein). The gradual mode is attributed to an increase in point defects. This gradual degradation, which takes place on a time-scale of 10 years, is responsible for a loss of efficiency. Moreover, all three modes are associated with thermal effects, but this link is not well understood.

There has recently been a considerable amount of work directed at the understanding of this heating process. Two-dimensional (transverse and lateral) steady-state results have been obtained for the system of equations given by electrical models (electron continuity, hole continuity and Poisson's equation), optical models (wave equation and photon rate equation) and thermal models (heat equation); see, for example, [5], [6]. These space-dependent models are currently exclusively solved by numerical approaches, despite the wide variation of length-scales. The numerical simulations require extensive computer resources, especially when parameter studies are required.

A fully lumped model, which comprises four ordinary differential equations, has recently been reported [7]. Asymptotic solutions of this lumped model explain the link between thermal effects and loss of efficiency. However, the steady-state temperature is a monotonic function of the current and spatial variation of thermal effects cannot be described. Subsequently we introduced a one-dimensional model, which comprises four partial differential equations

and one parametric ordinary differential equation, to describe the longitudinal variation of thermal effects [8]. Asymptotic solutions of this model have been obtained on the short and long thermal time-scales as with the lumped model. The increase in the density of point defects at the mirror (corresponding to degradation) produces a hot-spot over the short length-scale (in comparison to the cavity length) associated with the thermal conduction. The maximum steady-state temperature (in the hot-spot) is a monotonic function of current.

The purpose of this paper is to gain a better understanding of the failure mechanisms for semiconductor lasers. We extend the work done on hot-spots by considering the effect of a new scaling for the higher current, the higher photon density, the higher density of defects and the higher temperature. These new scalings result in a highly nonlinear boundary value problem to describe the steady-state temperature in the hot-spot. This equation admits a maximum temperature which is a multi-valued function of current. A result which explains the runaway phenomenon seen experimentally when the current is increased [4].

This paper is not concerned with the reduction of light intensity which may be explained by the temperature dependence of the threshold current

The contents of this paper will now be outlined. A one-dimensional model is formulated in Section II. These equations are non-dimensionalised in Section III. In Section IV, an asymptotic analysis of the model on thermal time-scales is undertaken. Section V examines the highly nonlinear boundary value problem which describes the maximum temperature at steady state. Section VI describes a numerical solution of the full system of equations to illustrate the predictions of the analysis. Finally, Section VII briefly draws some conclusions.

II. PROBLEM FORMULATION

This section outlines the inclusion of thermal effects into the travelling-wave rate equations (see [9]). We have

$$\frac{\partial N}{\partial t} = \frac{J}{ed} - a\left(N - N_t \exp(-E_{int}/k_B T_1)\right)\left(I^+ + I^-\right) \\ -N\left(A_{nr}\exp(-E_1/k_B T_1) + BN\exp(-E_2/k_B T_1) + CN^2\exp(-E_3/k_B T_1)\right), \tag{1}$$

$$\frac{\partial I^\pm}{\partial t} \pm \frac{c}{\mu_g}\frac{\partial I^\pm}{\partial z} = \left[a\left(N - N_t\exp(-E_{int}/k_B T_1)\right) - \frac{c\alpha_{int}}{\mu_g}\right] I^\pm + \beta B N^2 \exp(-E_2/k_B T_1), \tag{2}$$

where $N(z,t)$ is the concentration of electrons in the conduction band, $I^+(z,t)$ is the light intensity of the wave travelling in the positive z direction and $I^-(z,t)$ is the light intensity of the wave travelling in the negative z direction, t is time, z is the axial length, the constant J is the current density per unit axial length, e is the charge on an electron,

d is the thickness of the active layer, c is the velocity of light in a vacuum and μ_g is the group refractive index of the active layer.

In (1)–(2) the optical gain has been modelled by an expression of the form $G(N,T_1) = a(N - N_t \exp(-E_{int}/k_B T_1))$ where a is the linear gain rate, k_B is Boltzmann's constant, T_1 is the temperature per unit axial length of the active layer, E_{int} is the activation energy and $N_t e^{-E_{int}/k_B T_1}$ is the electron density at transparency. The linear dependence of the optical gain on the carrier density and the Arrhenius temperature dependence of absorption are adopted on the basis of the experimental evidence (see [10] and [11], respectively). We neglect any temperature dependence of a (*cf.* [5]).

The carrier lifetime, τ_c, is given by (see [7]) $1/\tau_c = A_{nr}(z)\exp(-E_1/k_B T_1) + BN\exp(-E_2/k_B T_1) + CN^2\exp(-E_3/k_B T_1)$ where $A_{nr}(z)$ is a function (discussed below) and B and C are constant. The first term on the right-hand side represents surface and defect recombination with activation energy E_1, the second radiative recombination with activation energy E_2 and the third Auger recombination with activation energy E_3. The radiative recombination can be split into spontaneous emission which enters the lasing mode and spontaneous emission which is absorbed in the surround as heat. The constant β represents the fraction of spontaneous radiation which enters the lasing mode. The electrons lost to the valence band by nonradiative and Auger recombination are assumed to have converted their energy into heat in the active layer.

The function $A_{nr}(z)$ represents the defects in the semiconductor caused by degradation. The rate of degradation is governed by mechanisms such as oxidation and fatigue. In general these processes are temperature dependent and take place over much larger time-scales (10 years) than those considered here; a typical model being an Arrhenius law (see (3.37) of [4]). The association of degradation with thermal effects indicates that it is appropriate to consider it on the thermal length-scale. This is in contrast to surface defects which are usually assumed to be on the molecular length-scale. The function $A_{nr}(z)$ will be assumed to be of the form

$$A_{nr}(z) = A_e \begin{cases} 1 + S(z) & z \leq \gamma, \\ 1 & \gamma < z < L - \gamma, \\ 1 + S(L - z) & L - \gamma \leq z, \end{cases}$$

where L is the cavity length, $S(z)$ represents the increased density of defects in the neighbourhood of the surface, γ is the penetration depth of these defects and A_e is the density of defects in the cavity of the laser. The defects will be taken to be of the form $S(z) = \alpha(\gamma - z)/\gamma$ where α represents a measure of the maximum density of defects. In the analysis which follows, we also take the slightly simpler form $S(z) = \alpha$ in order to obtain asymptotic solutions.

The rate of scattering loss at heterostructure interfaces is given by $c\alpha_{int}/\mu_g$ where α_{int} is the absorption constant. The photons in the lasing mode which are scattered at heterostructure interfaces are all assumed to be turned into heat in the surround. In the absence of experimental data, we neglect any temperature dependence of β and μ_g.

Thermal effects can then be coupled into the single-mode rate equations via

$$\rho_1 c_1 \frac{\partial T_1}{\partial t} - \frac{\partial}{\partial z}\left(k_1 \frac{\partial T_1}{\partial z}\right) = \left(A_{nr}\exp(-E_1/k_B T_1) + CN^2\exp(-E_3/k_B T_1)\right) NE_g + \frac{\kappa_1}{\Omega_1}(T_2 - T_1), \tag{3}$$

$$\rho_2 c_2 \frac{\partial T_2}{\partial t} - \frac{\partial}{\partial z}\left(k_2 \frac{\partial T_2}{\partial z}\right) = \frac{c\alpha_{int}E_g\Omega_1}{\mu_g\Omega_2}(I^+ + I^-) + (1-2\beta)\frac{BN^2E_g\Omega_1}{\Omega_2}\exp(-E_2/k_B T_1)$$

$$+\frac{\kappa_1}{\Omega_2}(T_1 - T_2) + \frac{\kappa_2}{\Omega_2}(T_a - T_2), \tag{4}$$

where ρ_1 is the density, c_1 the specific heat capacity and k_1 the thermal conductivity of the active layer, E_g is the band-gap energy, κ_1 is the heat transfer coefficient between the active and the surrounding layers, T_2 is the temperature per unit axial length, ρ_2 the density, c_2 the specific heat capacity and k_2 the thermal conductivity of the surrounding layer, κ_2 is the heat transfer coefficient between the surrounding layer and the material outside the laser, T_a is the (constant) ambient temperature, Ω_1 is the cross-sectional area of the active layer and Ω_2 is the cross-sectional area of the surround. The first term on the right-hand side of (3) is the energy generated by the nonradiative recombination of electrons and holes in the active region. The first term on the right-hand side of (4) represents the heat generated from the absorption of the scattering loss at heterostructure interfaces. The second term on the right-hand side of (4) represents the heat generated from the absorption of the spontaneous emission which deviates outside the active region. The remaining terms on the right-hand side of (3) and (4) model the transport of heat.

The boundary conditions for the intensities are given in terms of the reflectivities $R^{(1)}$ at $z = 0$ and $R^{(2)}$ at $z = L$ by the expressions

$$I^+(0,t) = R^{(1)}I^-(0,t), \qquad I^-(L,t) = R^{(2)}I^+(L,t). \tag{5}$$

Radiation and convection through the sides of the laser are assumed to be negligible, so we have

$$\frac{\partial T_1}{\partial z}(0,t) = \frac{\partial T_1}{\partial z}(L,t) = \frac{\partial T_2}{\partial z}(0,t) = \frac{\partial T_2}{\partial z}(L,t) = 0. \tag{6}$$

We neglect any temperature dependence of $R^{(1)}$ and $R^{(2)}$. Further details of the modelling are given in [8].

The threshold current ($J_{th}(T_1)$) and electron concentration at threshold ($N_{th}(T_1)$) are given by the solutions of the equations

$$\frac{c}{2\mu_g}\ln\left(\frac{1}{R^{(1)}R^{(2)}}\right)=\int_{z=0}^{L}a\left(N_{th}(T_1)-N_t\exp(-E_{int}/k_BT_1)\right)-\frac{c\alpha_{int}}{\mu_g}dz,$$

$$\frac{J_{th}(T_1)}{ed}=A_{nr}N_{th}(T_1)\exp(-E_1/k_BT_1)+BN_{th}(T_1)^2\exp(-E_2/k_BT_1)+CN_{th}(T_1)^3\exp(-E_3/k_BT_1).$$

The ratio of two threshold currents at different temperatures is given by

$$\frac{J_{th}(T_1)}{J_{th}(T_a)}=\frac{A_{nr}N_{th}(T_1)\exp\left(\frac{-E_1}{k_BT_1}\right)+BN_{th}(T_1)^2\exp\left(\frac{-E_2}{k_BT_1}\right)+CN_{th}(T_1)^3\exp\left(\frac{-E_3}{k_BT_1}\right)}{A_{nr}N_{th}(T_a)\exp\left(\frac{-E_1}{k_BT_a}\right)+BN_{th}(T_a)^2\exp\left(\frac{-E_2}{k_BT_a}\right)+CN_{th}(T_a)^3\exp\left(\frac{-E_3}{k_BT_a}\right)}.$$

An approximation for the characteristic temperature needs to be extracted from the right-hand side of this equation for each laser.

III. NON-DIMENSIONALISATION

We define N_e and I_e to be representative values for the average electron concentration and the average photon density at fixed temperature $T_1=T_a$ and current greater than the threshold current (described in [8]). The values of N_e and I_e are calculated using the formulas $N_e=N_t\exp(-E_{int}/k_BT_a)+c\left[\alpha_{int}+\ln\left(1/R_1R_2\right)/(2L)\right]/a\mu_g$ and

$$I_e=\frac{\frac{J}{ed}-A_{nr}\exp(-E_1/k_BT_a)N_e-B\exp(-E_2/k_BT_a)N_e^2-C\exp(-E_3/k_BT_a)N_e^3}{2a\left(N_e-N_t\exp(-E_{int}/k_BT_a)\right)}. \tag{7}$$

We define Δ to be a typical steady-state value of the active region temperature rise and calculate it from the formula $\Delta=\Omega_1N_eE_g\left(A_{nr}\exp(-E_1/k_BT_a)+CN_e^2\exp(-E_3/k_BT_a)\right)/\kappa_1$.

We introduce a time-scale τ_t which will be chosen shortly. Making the transformation to dimensionless variables $N=N_e\hat{N}$, $I^{\pm}=I_e\hat{I}^{\pm}$, $A_{nr}=A_e\hat{A}$, $T_1=T_a+\Delta\hat{T}_1$, $T_2=T_a+\Delta\hat{T}_2$, $z=L\hat{z}$ and $t=\tau_t\hat{t}$, equations (1)–(6) become

$$\lambda\frac{\partial\hat{N}}{\partial\hat{t}}=\frac{\mathcal{A}}{\Gamma}-\frac{\mathcal{B}}{\Gamma}\hat{g}(\hat{N},\hat{T}_1)\left(\hat{I}^{+}+\hat{I}^{-}\right)-\left(a_1\hat{A}\hat{N}\hat{f}(-A_1,\hat{T}_1)+a_2\hat{N}^2\hat{f}(-A_2,\hat{T}_1)+a_3\hat{N}^3\hat{f}(-A_3,\hat{T}_1)\right), \tag{8}$$

$$\lambda\frac{\partial\hat{I}^{\pm}}{\partial\hat{t}}\pm\frac{\mathcal{D}}{\nu}\frac{\partial\hat{I}^{\pm}}{\partial\hat{z}}=\frac{1}{\nu}\left[\hat{g}(\hat{N},\hat{T}_1)-\mathcal{E}\right]\hat{I}^{\pm}+\Gamma\mathcal{G}\hat{N}^2\hat{f}(-A_2,\hat{T}_1), \tag{9}$$

$$\frac{\partial\hat{T}_1}{\partial\hat{t}}-\sigma^2\frac{\partial^2\hat{T}_1}{\partial\hat{z}^2}=\mathcal{K}\hat{A}\hat{N}\hat{f}(-A_1,\hat{T}_1)+\mathcal{L}\hat{N}^3\hat{f}(-A_3,\hat{T}_1)+\hat{T}_2-\hat{T}_1, \tag{10}$$

$$\frac{\partial\hat{T}_2}{\partial\hat{t}}-\mathcal{S}\varepsilon\frac{\partial^2\hat{T}_2}{\partial\hat{z}^2}=\mathcal{N}\varepsilon\left(\hat{I}^{+}+\hat{I}^{-}\right)+\mathcal{P}\varepsilon\hat{N}^2\hat{f}(-A_2,\hat{T}_1)+\mathcal{Q}\varepsilon(\hat{T}_1-\hat{T}_2)-\varepsilon\hat{T}_2, \tag{11}$$

where $\hat{f}(\Lambda,\hat{T}_1)=\exp\left\{\Lambda/(1+\delta\hat{T}_1)\right\}$ and $\hat{g}(\hat{N},\hat{T}_1)=\hat{N}-N^*\hat{f}(\Gamma\hat{T}_1,\hat{T}_1)$ with the boundary conditions

$$\hat{I}^+(0,\hat{t}) = R^{(1)}\hat{I}^-(0,\hat{t}), \quad \hat{I}^-(1,\hat{t}) = R^{(2)}\hat{I}^+(1,\hat{t}), \quad \frac{\partial \hat{T}_1}{\partial \hat{z}}(0,\hat{t}) = \frac{\partial \hat{T}_1}{\partial \hat{z}}(1,\hat{t}) = \frac{\partial \hat{T}_2}{\partial \hat{z}}(0,\hat{t}) = \frac{\partial \hat{T}_2}{\partial \hat{z}}(1,\hat{t}) = 0. \tag{12}$$

The dimensionless constants $\mathcal{A}/\Gamma$, a_1, a_2, a_3, A_1, A_2, A_3, $\mathcal{B}/\Gamma$, N^*, Γ, δ, ν, $\mathcal{D}/\nu$, $\mathcal{E}/\nu$, $\mathcal{G}\Gamma$, $\mathcal{K}$, $\mathcal{L}$, λ, σ^2, $\mathcal{N}\varepsilon$, $\mathcal{P}\varepsilon$, $\mathcal{Q}\varepsilon$, ε, $R^{(1)}$, $R^{(2)}$ and $\mathcal{S}\varepsilon$ are defined in Table I; the time-scale chosen being $\tau_t = \rho_1 c_1 \Omega_1/\kappa_1$, giving a balance between the rate of change of temperature of the active region and the Newton cooling term. The electrical time-scale is defined by $\tau_e = 1/A_e$ (the longest of the two time-scales on the right-hand side of (8)). The conditions $\nu \ll 1$, $\lambda \ll 1$, $\varepsilon \ll 1$, $\Gamma \ll 1$, $\sigma \ll 1$, $\delta/\Gamma \ll 1$ typically hold in practice. The small parameters are ν, representing the ratio of the optical time-scale to the electrical time-scale; λ, the ratio of the electrical to the short thermal time-scale; ε, the ratio of the short thermal time-scale to the long thermal time-scale; σ, the ratio of the thermal boundary layer length-scale to the cavity length; δ, the typical temperature rise in the active region relative to the ambient temperature; and Γ, the dimensionless activation energy for absorption. The value of the applied current (J) and the corresponding photon density (I_e; see (7)) justify the choice of scaling for the dimensionless constants $\mathcal{A}/\Gamma$, $\mathcal{B}/\Gamma$ and $\mathcal{G}\Gamma$; this choice producing the appropriate balance in the analysis which follows. These small parameters will be exploited in simplifying the thermal problem in Section IV.

IV. ASYMPTOTIC ANALYSIS

A. Introduction

There are several disparate time-scales and two length-scales in the problem (8)–(12). We study these equations on the short ($\hat{t} = O(1)$) and long ($\hat{t} = O(1/\varepsilon)$) thermal time-scales. Both of the length-scales are required in the analysis which follows.

The leading order term for temperature in [8] satisfied an outer problem and an inner problem close to the mirror facet. The extra term introduced in the boundary layer corresponded to axial thermal conduction. The temperature was much higher in the boundary layer than in the body of the semiconductor due to the heating mechanism associated with defects in the neighbourhood of the surface, the boundary layer being described as a hot-spot. As the current is increased, the temperature in the hot-spot also increases. The temperature dependence of the absorption, which was previously treated as a lower order term [8], now enters the leading order problem. This new balance requires a new layer in which the temperature and the number of defects are scaled in terms of the small parameter Γ. In summary, the leading order problem on the thermal time-scales comprises an outer problem and two layers close to the mirror

facet.

B. Short thermal time-scale

1. Outer expansion

The required expansions take the form $\hat{N} \sim N_0$, $\hat{I}^+ \sim F_0$, $\hat{I}^- \sim B_0$, $\hat{T}_1 \sim T_0^{(1)}$ and $\hat{T}_2 = O(\varepsilon)$. We obtain

$$F_0 = C \exp\left(\int_{x=0}^{\hat{z}} [N_0 - N^* - \mathcal{E}]\, dx/\mathcal{D}\right), \qquad B_0 = C\sqrt{\frac{R^{(2)}}{R^{(1)}}} \exp\left(\int_{x=\hat{z}}^{1} [N_0 - N^* - \mathcal{E}]\, dx/\mathcal{D}\right),$$

and N_0 given by

$$\mathcal{B}\,(N_0 - N^*)\,(F_0 + B_0) = \mathcal{A}, \tag{13}$$

where ($C \neq 0$ because $\mathcal{A} \neq 0$)

$$\frac{1}{2}\ln\left(\frac{1}{R^{(1)}R^{(2)}}\right) = \int_{x=0}^{1} [N_0 - N^* - \mathcal{E}]\, dx/\mathcal{D}. \tag{14}$$

Equation (10) implies the general solution $T_0^{(1)} = \left[\mathcal{K}\hat{A}N_0 \mathrm{e}^{-A_1} + \mathcal{L}N_0^3 \mathrm{e}^{-A_3}\right] + g(\hat{z})e^{-\hat{t}}$. Therefore, the steady state in this outer problem is stable for all choices of initial condition consistent with these scalings. The first term in the expansion for $\hat{T}_1$ does not satisfy the boundary conditions, in general, and there are boundary layers at $\hat{z} = 0$ and $\hat{z} = 1$. We consider the layers at $\hat{z} = 0$ in the following two subsections; the layers at $\hat{z} = 1$ being similar.

2. Layer I at $\hat{z} = 0$

We perform the stretching transformation $\hat{z} = \sigma Z_1$ in the boundary layer and let $\hat{N} \sim n_0$, $\hat{I}^+ \sim f_0$, $\hat{I}^- \sim b_0$, $\hat{T}_1 \sim \theta_0/\Gamma$, $\hat{T}_2 = O(\varepsilon)$ and $\hat{A} \sim A_0/\Gamma$. The scaling on $\hat{A}$ corresponds to the increased density of defects in the neighbourhood of the surface. Equation (9) implies $f_0 = F_0(0)$, $b_0 = B_0(0)$ and (8) then gives

$$n_0 = \frac{\mathcal{A} + \mathcal{B}N^* \exp(\theta_0)\,(f_0 + b_0)}{a_1 A_0 \exp(-A_1) + \mathcal{B}\,(f_0 + b_0)}.$$

We thus obtain

$$\frac{\partial \theta_0}{\partial \hat{t}} + \theta_0 - \frac{\partial^2 \theta_0}{\partial Z_1^2} = \mathcal{K}A_0 \exp(-A_1)\left\{\frac{\mathcal{A} + \mathcal{B}N^* \exp(\theta_0)\,(f_0 + b_0)}{a_1 A_0 \exp(-A_1) + \mathcal{B}\,(f_0 + b_0)}\right\} \tag{15}$$

with one boundary condition at $Z_1 = 0$ given by $\partial\theta_0/\partial Z_1 = 0$ and the other to be determined by matching. We note that the exponential nonlinearity on the right-hand side of (15) was not present in the asymptotic analysis of [8].

3. Layer II at $\hat{z} = 0$

We perform the stretching transformation $\hat{z} = \sigma(\ln(1/\Gamma) + Z_2)$ in the boundary layer and let $\hat{N} \sim \bar{n}_0$, $\hat{I}^+ \sim f_0$, $\hat{I}^- \sim b_0$, $\hat{T}_1 \sim \psi_0$ and $\hat{T}_2 = O(\varepsilon)$. Equation (8) implies $\bar{n}_0 = (\mathcal{A} + \mathcal{B}N^*(f_0 + b_0))/\mathcal{B}(f_0 + b_0)$ and (10) then gives

$$\frac{\partial \psi_0}{\partial \hat{t}} + \psi_0 - \frac{\partial^2 \psi_0}{\partial Z_2^2} = \mathcal{K}\hat{A}\bar{n}_0 \exp(-A_1) + \mathcal{L}\bar{n}_0^3 \exp(-A_3)$$

with boundary conditions determined from matching with layer I and the outer expansion.

C. Long thermal time-scale

This corresponds to the time-scale of conduction in the surround and is the longest time-scale in the problem. In (8)–(11) we scale $\hat{t} = \tau/\varepsilon$ to give

$$\lambda\varepsilon\frac{\partial \hat{N}}{\partial \tau} = \frac{\mathcal{A}}{\Gamma} - \frac{\mathcal{B}}{\Gamma}\hat{g}(\hat{N}, \hat{T}_1)\left(\hat{I}^+ + \hat{I}^-\right) - \left(a_1\hat{A}\hat{N}\hat{f}(-A_1, \hat{T}_1) + a_2\hat{N}^2\hat{f}(-A_2, \hat{T}_1) + a_3\hat{N}^3\hat{f}(-A_3, \hat{T}_1)\right), \tag{16}$$

$$\lambda\varepsilon\frac{\partial \hat{I}^\pm}{\partial \tau} \pm \frac{\mathcal{D}}{\nu}\frac{\partial \hat{I}^\pm}{\partial \hat{z}} = \frac{1}{\nu}\left[\hat{g}(\hat{N}, \hat{T}_1) - \mathcal{E}\right]\hat{I}^\pm + \Gamma\mathcal{G}\hat{N}^2\hat{f}(-A_2, \hat{T}_1), \tag{17}$$

$$\varepsilon\frac{\partial \hat{T}_1}{\partial \tau} - \sigma^2\frac{\partial^2 \hat{T}_1}{\partial \hat{z}^2} = \mathcal{K}\hat{A}\hat{N}\hat{f}(-A_1, \hat{T}_1) + \mathcal{L}\hat{N}^3\hat{f}(-A_3, \hat{T}_1) + \hat{T}_2 - \hat{T}_1, \tag{18}$$

$$\frac{\partial \hat{T}_2}{\partial \tau} - \mathcal{S}\frac{\partial^2 \hat{T}_2}{\partial \hat{z}^2} = \mathcal{N}\left(\hat{I}^+ + \hat{I}^-\right) + \mathcal{P}\hat{N}^2\hat{f}(-A_2, \hat{T}_1) + \mathcal{Q}(\hat{T}_1 - \hat{T}_2) - \hat{T}_2. \tag{19}$$

1. Outer Expansion

The required expansions take the form $\hat{N} \sim N_0$, $\hat{I}^+ \sim F_0$, $\hat{I}^- \sim B_0$, $\hat{T}_1 \sim \Phi_0^{(1)}$ and $\hat{T}_2 \sim \Phi_0^{(2)}$. Equation (18) implies $\mathcal{K}\hat{A}N_0\mathrm{e}^{-A_1} + \mathcal{L}N_0^3\mathrm{e}^{-A_3} + \Phi_0^{(2)} - \Phi_0^{(1)} = 0$, and (19) then gives

$$\frac{\partial \Phi_0^{(2)}}{\partial \tau} + \Phi_0^{(2)} - \mathcal{S}\frac{\partial^2 \Phi_0^{(2)}}{\partial \hat{z}^2} = -p(\hat{z}) \quad \text{with} \quad \frac{\partial \Phi_0^{(2)}}{\partial \hat{z}}(0, \tau) = \frac{\partial \Phi_0^{(2)}}{\partial \hat{z}}(1, \tau) = 0,$$

where $p(\hat{z}) = -\mathcal{N}(F_0 + B_0) - \mathcal{P}N_0^2\mathrm{e}^{-A_2} - \mathcal{Q}\left\{\mathcal{K}\hat{A}N_0\mathrm{e}^{-A_1} + \mathcal{L}N_0^3\mathrm{e}^{-A_3}\right\}$. We obtain

$$\Phi_0^{(2)}(\hat{z}, \tau) = \sum_{n=0}^{\infty} A_n \exp\{-(1 + \mathcal{S}n^2\pi^2)\tau\}\cos(n\pi\hat{z}) + \int_{\xi=0}^{1} G(\xi, \hat{z})p(\xi)d\xi,$$

where

$$G(\xi,\hat{z}) = \frac{1}{\sqrt{S}} \begin{cases} \cosh(\xi/\sqrt{S}) \left(\sinh(\hat{z}/\sqrt{S}) - \cosh(\hat{z}/\sqrt{S}) \coth(1/\sqrt{S}) \right) & \xi < \hat{z}, \\ \cosh(\hat{z}/\sqrt{S}) \left(\sinh(\xi/\sqrt{S}) - \cosh(\xi/\sqrt{S}) \coth(1/\sqrt{S}) \right) & \hat{z} < \xi. \end{cases}$$

and A_n are determined by matching with the short thermal time-scale. The steady state in this outer problem is stable for all choices of initial condition consistent with these scalings. We now consider the boundary layers at $\hat{z} = 0$ in a similar manner to the short thermal time-scale.

2. Layer A at $\hat{z} = 0$

We perform the stretching transformation $\hat{z} = \sigma Z_1$ in the boundary layer and let $\hat{N} \sim \eta_0$, $\hat{I}^+ \sim f_0$, $\hat{I}^- \sim b_0$, $\hat{T}_1 \sim \Theta_0/\Gamma$, $\hat{T}_2 = O(1)$ and $\hat{A} \sim A_0/\Gamma$. Equation (16) implies

$$\eta_0 = \frac{\mathcal{A} + \mathcal{B}N^* \exp(\Theta_0)\,(f_0 + b_0)}{a_1 A_0 \exp(-A_1) + \mathcal{B}\,(f_0 + b_0)}.$$

We thus obtain

$$\Theta_0 - \frac{\partial^2 \Theta_0}{\partial Z_1^2} = \mathcal{K} A_0 \exp(-A_1) \left\{ \frac{\mathcal{A} + \mathcal{B}N^* \exp(\Theta_0)\,(f_0 + b_0)}{a_1 A_0 \exp(-A_1) + \mathcal{B}\,(f_0 + b_0)} \right\} \tag{20}$$

with one boundary condition at $Z_1 = 0$ given by $\partial\Theta_0/\partial Z_1 = 0$ and the other to be determined by matching. We again note the exponential nonlinearity on the right-hand side of (20).

3. Layer B at $\hat{z} = 0$

We perform the stretching transformation $\hat{z} = \sigma(\ln(1/\Gamma) + Z_2)$ in the boundary layer and let $\hat{N} \sim \bar{n}_0$, $\hat{I}^+ \sim f_0$, $\hat{I}^- \sim b_0$, $\hat{T}_1 \sim \Psi_0^{(1)}$ and $\hat{T}_2 \sim \Psi_0^{(2)}$. Equation (19) implies $\Psi_0^{(2)} = \Phi_0^{(2)}(0,\tau)$ and (18) then gives

$$\Psi_0^{(1)} - \frac{\partial^2 \Psi_0^{(1)}}{\partial Z_2^2} = \mathcal{K}\hat{A}\bar{n}_0 \exp(-A_1) + \mathcal{L}\bar{n}_0^3 \exp(-A_3) + \Psi_0^{(2)}$$

with boundary conditions determined from matching with layer A and the outer expansion.

V. THERMAL RUNAWAY

A. Introduction

In this section we examine the maximum value of temperature at steady state. Moreover, we are interested in treating $\mathcal{A}$ as a bifurcation parameter which corresponds to varying the current. In [8], the maximum temperature

at steady state is a monotonic function of current and this does not explain the phenomenon of thermal runaway. The additional nonlinearities, which are introduced in layer I and layer A, admit a maximum temperature which is a multi-valued function of current.

We now derive the equation which describes the dependence of the maximum temperature on $\mathcal{A}$, utilising the equations for the short or long thermal time-scales in Section IV. We use (13) to eliminate the photon densities from (15) or (20) and note that the function $A_0(Z_1)$ is only non-zero over a finite length, namely $[0, W)$. For $Z_1 \geq W$, the steady-state temperature, $\theta(Z_1)$, is given by $\theta = Pe^{-Z_1} + Qe^{Z_1}$ where P and Q are constants. Matching with layer II implies that $Q = 0$. Therefore we can prescribe the boundary condition at $Z_1 = W$ by $\mathrm{d}\theta/\mathrm{d}Z_1 = -\theta$. We summarise the nonlinear boundary value problem which describes the maximum temperature as follows

$$\frac{\mathrm{d}^2\theta}{\mathrm{d}Z_1^2} = \theta - \bar{k}A_0\mathcal{A}\left\{\frac{\bar{N} + N^* \exp(\theta)}{\bar{a}\bar{N}A_0 + \mathcal{A}}\right\} \tag{21}$$

where $\bar{a} = a_1 \exp(-A_1)$, $\bar{k} = \mathcal{K}\exp(-A_1)$ and $\bar{N} = N_0(0) - N^*$ with boundary conditions

$$\text{at } Z_1 = 0 \quad \frac{\mathrm{d}\theta}{\mathrm{d}Z_1} = 0, \text{ at } Z_1 = W \quad \frac{\mathrm{d}\theta}{\mathrm{d}Z_1} = -\theta. \tag{22}$$

The quantity $N_0(0)$ is taken to be fixed because the physical solutions of (13)–(14) corresponds to $\mathcal{A}/C$ constant and N_0 independent of the choice of $\mathcal{A}$. In this section, we consider four examples of (21)–(22) for different functions $A_0(Z_1)$ and constants W. In two cases, we will obtain numerical results with the AUTO bifurcation package and, in the other two cases, we will make asymptotic simplifications.

B. $W = O(1)$, $A_0 = \chi(W - Z_1)$

Firstly we consider a particular version of (21)–(22) with $A_0 = 4(1 - Z_1)$, $W = 1$ and the data given in Table I (the reason for the choice $\chi = 4$ will become apparent). The maximum value of θ at steady state as a function of the bifurcation parameter $\mathcal{A}$ is shown in Figure 2. It is clear from the figure that there is a current $\mathcal{A}_c$, beyond which no bounded steady state exists; that is, more power is deposited by non-radiative recombination than is lost by thermal conduction. The nonexistence of bounded solutions beyond the critical current is mathematically a consequence of the uniform intensity within the boundary layer and the assumption of Arrhenius temperature dependence in the expression for absorption. The upper branch of the response curve becomes invalid as $\theta \to \infty$ because at these high temperatures the absorption becomes very large and the intensity may no longer be taken as uniform across the boundary layer. Numerical simulations of (8)–(12), with the appropriate choice of initial conditions, indicate that the lower branch is stable and the upper branch unstable.

We now examine the variation of the current, $\mathcal{A}_c$, beyond which no bounded steady state exists in response to changes in W and χ. The results of simulations with $W = 1$ and several values for χ are shown in Figure 3. For $\chi \ll 1$, the figure indicates that no fold bifurcation takes place, that is a bounded steady state solution always exists. However, for $\chi \gg 1$, the current $\mathcal{A}_c$ decreases significantly only leaving a narrow range of currents available for stable operation. We now consider the results of simulations with $\chi = 4$ and several values for W (shown in Figure 4). For $W \ll 1$, the figure indicates that a bounded steady state always exists. In the case $W \gg 1$, only a narrow range of currents are available for stable operation. This behaviour is consistent with experimental observations of the sudden mode of failure [4].

We also note that the maximum temperature is a multi-valued function of the density of defects in the neighbourhood of the surface. The response diagram for fixed $\mathcal{A} = 1$ with the bifurcation parameter χ is shown in Figure 5. The sudden mode of failure may be explained in terms of the slow increase in χ which takes place during aging. The sudden failure occurring as χ passes through χ_c the critical defect density beyond which no bounded steady state exists.

The current is proportional to the optical power at leading order. The response diagram with bifurcation parameter taken to be optical power is a scaled version of Figure 2.

C. $W = O(1)$, A_0 constant

We consider an autonomous version of (21)–(22) with $A_0 = 4$ and $W = 1$ for comparison. The response diagram is qualitatively similar to Figure 2. However, the increase in the number of defects produces a fold at the lower value of current ($\mathcal{A}_c \simeq 0.2$).

D. $W \ll 1$, A_0 constant

Consider the case where A_0 is taken to be a constant and $W \to 0$, then problem (21)–(22) is of regular perturbation type. We take $Z_1 = W\bar{Z}$. Two steady states arise: one given by

$$\theta \sim W\bar{\theta}_0 + W^2\bar{\theta}_1 \quad \text{where} \quad \bar{\theta}_0 = \frac{\bar{k}(\bar{N} + N^*)A_0\mathcal{A}}{\bar{a}\bar{N}A_0 + \mathcal{A}}$$

and the other given by

$$\theta \sim \ln(1/W) + \ln\ln(1/W) + \tilde{\theta}_0 + W\ln(1/W)\tilde{\theta}_1 \quad \text{where} \quad \tilde{\theta}_0 = \ln\left(\frac{\bar{a}\bar{N}A_0 + \mathcal{A}}{\bar{k}A_0\mathcal{A}N^*}\right).$$

The axial thermal conduction balances with the thermal source term, the transverse and lateral thermal conduction only appears at lower order. We note that no fold bifurcation is present in the response diagram in this case.

E. $W \gg 1$, A_0 constant

For $W \to \infty$ and A_0 taken to be a constant, problem (21)–(22) is of singular perturbation type. The transverse and lateral thermal conduction balances with the thermal source term in the outer problem, the axial thermal conduction only plays a part in the inner expansion. We take $Z_1 = WZ$.

Outer Expansion. The required outer expansion takes the form $\theta \sim \bar{\phi}_0$ which satisfies the nonlinear algebraic equation

$$\bar{\phi}_0 = \bar{k} A_0 \mathcal{A} \left\{ \frac{\bar{N} + N^* \exp(\bar{\phi}_0)}{\bar{a}\bar{N}A_0 + \mathcal{A}} \right\}.$$

The fold point, $\mathcal{A} = \mathcal{A}_c$, is given by the unique positive real root of the equation $\Upsilon N^* \exp(\Upsilon \bar{N} + 1) = 1$ where $\Upsilon = \bar{k} A_0 \mathcal{A}_c / (\bar{a}\bar{N}A_0 + \mathcal{A}_c)$. This outer solution does not satisfy the boundary condition at $Z = 1$ and there exists a boundary layer. The transverse and lateral thermal conduction balances with the thermal source term in this outer expansion, the axial thermal conduction will appear in the boundary layer.

Inner Expansion. We rescale the independent variable $Z = 1 - \xi/W$ and introduce an expansion of the form $\theta \sim \bar{\Phi}_0(\xi)$. We obtain

$$\frac{\mathrm{d}^2 \bar{\Phi}_0}{\mathrm{d}\xi^2} = \bar{\Phi}_0 - \bar{k} A_0 \mathcal{A} \left\{ \frac{\bar{N} + N^* \exp(\bar{\Phi}_0)}{\bar{a}\bar{N}A_0 + \mathcal{A}} \right\} \quad \text{with} \quad \text{at } \xi = 0 \quad \frac{\mathrm{d}\bar{\Phi}_0}{\mathrm{d}\xi} = \bar{\Phi}_0, \quad \frac{\mathrm{d}\bar{\Phi}_0}{\mathrm{d}\xi} \to 0 \quad \text{as } \xi \to \infty.$$

The response diagram for (21)–(22) with $W = 10$ and $A_0 = 4$ is again qualitatively similar to Figure 2. The increase in W produces a fold at a lower value of current than in Subsection V C ($\mathcal{A}_c \simeq 0.1$).

VI. NUMERICAL SOLUTION

We discretise the spatial variable in (8)–(11) leading to a system of ordinary differential equations. The convection terms in (9) are represented by a first-order upwind discretisation. The diffusion terms in equations (10)–(11) are approximated by the standard conservative central difference. The thermal diffusion coefficient in (10) is sufficiently small to only become significant in a thin region of space. We select a mesh which (i) accurately models the boundary

layers at $\hat{z} = 0$ and $\hat{z} = 1$ and (ii) varies continuously throughout the domain. We chose a Bakhvalov mesh (see [12] and references therein) in the regions $0 \leq \hat{z} < \gamma/L$ and $1 - \gamma/L < \hat{z} \leq 1$ to satisfy (i). We must be careful, in addressing (ii), not to significantly increase the number of mesh points. Define a uniform mesh $x_N, x_{N+1}, \ldots, x_{N+m}$ on $[-\pi/2, \pi/2]$ as the starting point. Then define a mapping $z_j = f(x_j)$, where $f(x) = 1/2 + (1/2 - \gamma/L)\sin(x)$, to produce a progressive refinement towards both boundary layers. The parameter values in Table I indicate that a number of very different time-scales are present and the stiff ordinary differential equation solver D02EAF was accordingly selected from the NAG library. Numerical results have been obtained for a variety of meshes but it was not possible to obtain grid independence in the simulation of thermal runaway owing to the ill-posed nature of the problem. However, the results did remain qualitatively the same on the various mesh refinements and we present the results to illustrate the analysis. The numerical simulations, which attained bounded steady states, proved to be grid independent.

We present the stable steady state attained for the parameter values given in Table I. The steady-state temperature rise in the active region is shown in Figure 6, higher temperatures being attained there than the surround. We note that the temperature rise in the surround does not exhibit the sharp maxima seen in the temperature rise of the active region. The maximum steady-state temperature rise in the active region predicted by the lower branch of the response diagram in Figure 2 is 13K, similarly a value of 13K is predicted by the numerical solution; the two approaches showing good agreement. As a result of the temperature rise, the light intensity (shown in Figure 7) decreases slightly. The electron concentration increases in response to these temperature rises with maxima being observed in the neighbourhood of both mirrors.

We now seek numerical results for the parameter values given in Table I except that we take $\mathcal{A} = 1$. This choice of parameter values corresponds to the régime where no bounded steady-state solutions exist (*cf.* Figure 2). The simulation is started from the initial condition $\hat{N}(\hat{z}, 0) = 0$, $\hat{I}^{\pm}(\hat{z}, 0) = 0$, $\hat{T}_1(\hat{z}, 0) = 0$ and $\hat{T}_2(\hat{z}, 0) = 0$. Numerical results are given for two spatial meshes: one in which there are 100 points within each Bakhvalov mesh and 280 points in total (mesh A) and one in which there are 80 points within each Bakhvalov mesh and 220 points in total (mesh B). The results are qualitatively the same for the two meshes. The temperature rise of the active region on the mirror facet as a function of time is shown in Figure 8. The temperature of the active region shows a gradual increase and this is accompanied by a gradual increase in electron concentration and a slow decrease in light intensity (shown in Figure 9). The rate of change of temperature in the active region increases rapidly as the temperature in the active region attains a value where nonlinear effects dominate. The high temperatures result in a sudden reduction of

photon density and increase in electron concentration at the mirror due to the strong temperature dependence of the absorption. The temperature rise in the active region and the surround as a function of longitudinal length is shown in Figure 10. The temperature rise in the boundary layer is significantly higher than inside the cavity of the laser.

VII. SUMMARY AND CONCLUSIONS

A mathematical model has been introduced to describe the thermal runaway observed during semiconductor laser operation. The equations are scaled to reflect the effect of high current, photon density, density of defects and temperature. An asymptotic analysis results in a stable steady state in the body of the laser and in a highly nonlinear boundary value problem to describe the steady-state temperature in the hot-spot. The response diagram for this boundary value problem takes the form of a fold in terms of the bifurcation parameter which represents current. Numerical simulations of the full time-dependent system determines that the lower branch is stable and the upper branch is unstable. (We may also choose the bifurcation parameter to be the density of defects in the neighbourhood of the surface and obtain a fold in the response diagram.) We note that fold bifurcations have structural stability. The fold bifurcations obtained for the leading-order equations will therefore be characteristic of the complete system of equations. The subsequent terms in the asymptotic expansions merely represent imperfections. Moreover, this general behaviour should also be observed in other (higher dimensional) models for semiconductor lasers with strong temperature dependence of the photon absorption.

The length-scale over which the increased density of defects stretches is an important parameter in determining the critical current beyond which no bounded steady states exist. If this distance is significantly less than the thermal length-scale ($\sqrt{k_1\Omega_1/\kappa_1}$) then there is a stable and an unstable steady state. Thermal runaway only takes place when extreme initial conditions are prescribed. In contrast if this length-scale is significantly greater than the thermal length-scale then there is only a narrow range of currents over which a stable steady state can be obtained. Similar comments apply to the magnitude of the increased density of defects in the neighbourhood of the facet relative to the reference value $A_e k_B T_a^2/E_{int}\Delta$.

We conclude by offering an explanation of the sudden mode of failure in terms of thermal runaway. The sudden mode corresponds to the device set-up initially lying inside the region where bounded steady states are allowed but the slow increase in defects (aging) moves the device parameters out of this region. The instant the device crosses this boundary a sudden increase in temperature takes place at the mirror facet and a sudden decrease in laser output. The temperature at the facet can exceed the melting point of the laser crystal leading to the so-called catastrophic

optical damage.

ACKNOWLEDGMENTS

Financial support for this work was provided by the EPSRC and the TMR network entitled 'Differential Equations in Industry and Commerce'. This project has benefited from the generous advice of J. R. King, B. Tuck and R. M. M. Mattheij.

---

[1] A. K. Kapila, *Asymptotic treatment of chemically reacting systems* (Pitman Advanced Publishing Program, Boston, 1983).

[2] G. A. Kriegsmann, J. Appl. Phys. **71**, 1960 (1992).

[3] A. A. Lacey, J. Comput. Appl. Math. **97**, 39 (1998).

[4] M. Fukuda, *Reliability and Degradation of Semiconductor Lasers and LEDs* (Artech House, Boston, 1991).

[5] G. Tan, N. Bewtra, K. Lee, and J. M. Xu, IEEE J. Quantum Electron. **29**, 822 (1993).

[6] M. Gault, P. Mawby, A. R. Adams, and M. Towers, IEEE J. Quantum Electron. **30**, 1691 (1994).

[7] W. R. Smith, J. R. King, B. Tuck, and J. W. Orton, IMA J. Appl. Math. **63**, 1 (1999).

[8] W. R. Smith, *Q. Jl Mech. Appl. Math.*, to appear.

[9] J. Z. Wilcox and L. W. Casperson, J. Appl. Phys. **56**, 57 (1984).

[10] P. M. Boers and M. T. Vlaardingerbroek, Electron. Lett. **11**, 206 (1975).

[11] C. H. Henry, P. M. Petroff, R. A. Logan, and F. R. Merritt, J. Appl. Phys. **50**, 3721 (1979).

[12] H. G. Roos, M. Stynes, and L. Tobiska, *Numerical Methods for Singularly Perturbed Differential Equations* (Springer-Verlag, Berlin, 1996).

TABLE I. Dimensionless parameters for a typical GaAs laser diode (where some values are reliable and some best estimates).

Symbol	Definition	Typical Value
$\mathcal{A}/\Gamma$	$J\tau_e/N_e ed$	8
α		3×10^2
a_1	$A_e\tau_e$	1
a_2	$BN_e\tau_e$	1
a_3	$CN_e^2\tau_e$	0.3
A_1	E_1/k_BT_a	1
A_2	E_2/k_BT_a	1
A_3	E_3/k_BT_a	1
$\mathcal{B}/\Gamma$	$aI_e\tau_e$	10
N^*	$N_t \exp(-E_{int}/k_BT_a)/N_e$	0.7
ν	$1/\ a\tau_eN_e$	1×10^{-4}
$\mathcal{D}/\nu$	$c\tau_e/\mu_gL$	2×10^3
$\mathcal{E}/\nu$	$c\alpha_{int}\tau_e/\mu_g$	1×10^3
$\mathcal{G}\Gamma$	$\beta BN_e^2\tau_e/I_e$	8×10^{-2}
γ/L		4×10^{-3}
$\mathcal{K}$	$A_eN_eE_g\tau_t/\rho_1c_1\Delta$	2
$\mathcal{L}$	$CN_e^3E_g\tau_t/\rho_1c_1\Delta$	0.5
$\mathcal{N}\varepsilon$	$c\alpha_{int}I_eE_g\tau_t\Omega_1/\mu_g\rho_2c_2\Delta\Omega_2$	3×10^{-4}
$\mathcal{P}\varepsilon$	$(1-2\beta)BN_e^2E_g\tau_t\Omega_1/\rho_2c_2\Delta\Omega_2$	2×10^{-4}
$\mathcal{Q}\varepsilon$	$\kappa_1\tau_t/\rho_2c_2\Omega_2$	1×10^{-4}
$R^{(1)}$		0.3
$R^{(2)}$		0.3
$\mathcal{S}\varepsilon$	$k_2\tau_t/\rho_2c_2L^2$	2×10^{-5}
Γ	$E_{int}\Delta/k_BT_a^2$	1×10^{-2}
δ	Δ/T_a	2×10^{-3}
λ	τ_e/τ_t	0.1
ε	$\rho_1c_1\Omega_1\kappa_2/\rho_2c_2\Omega_2\kappa_1$	6×10^{-4}
σ^2	$k_1\Omega_1/\kappa_1L^2$	2×10^{-5}

List of Figures

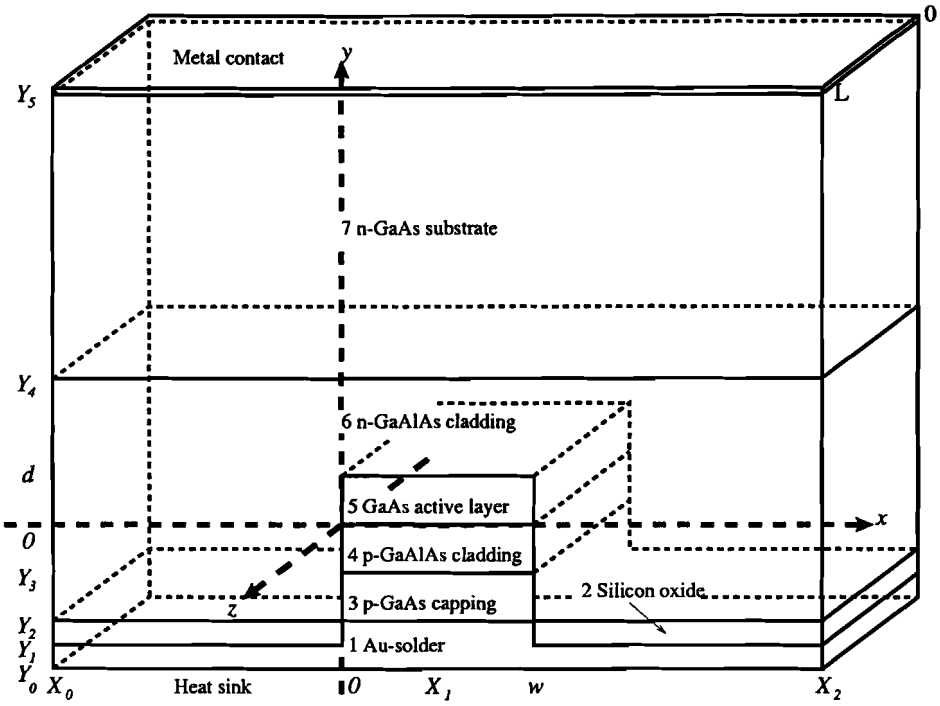

FIG. 1. Typical layered structure of a double-heterostructure semiconductor laser. The lateral direction is denoted by x, the transverse direction by y and the longitudinal (or axial) direction by z. The battery potential is applied in the transverse direction, the mirrors are located at $z = 0$ and $z = L$ and $X_1 = w/2$.

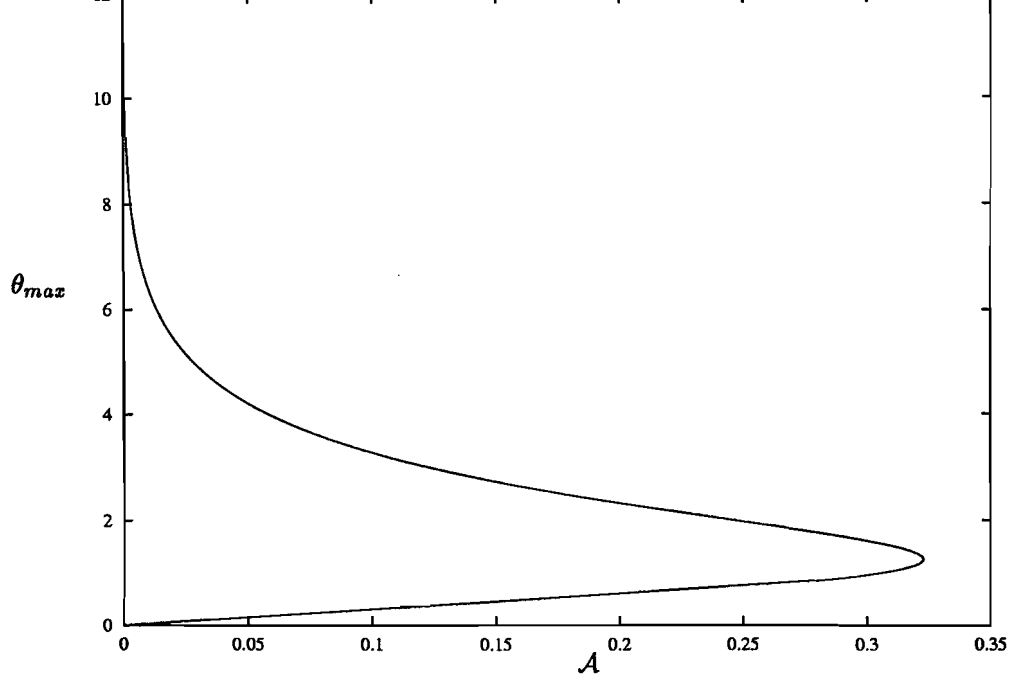

FIG. 2. Typical steady-state response diagram for the maximum temperature θ_{max} plotted against the bifurcation parameter $\mathcal{A}$. The parameter values are given in Table I with $A_0 = 4(W - Z_1)$ and $W = 1$.

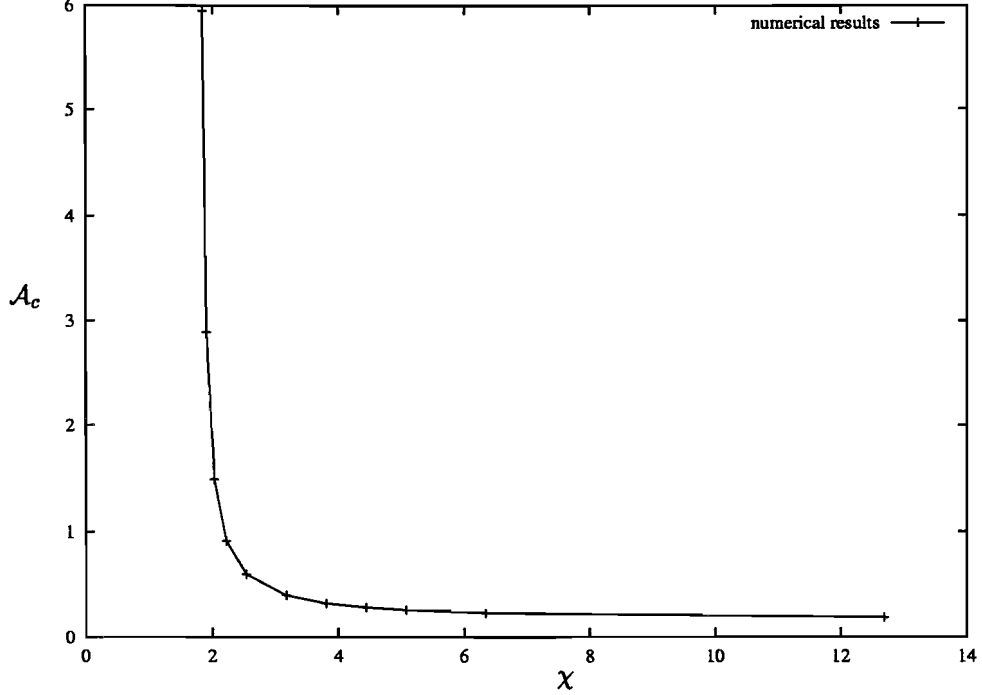

FIG. 3. The decrease in the current beyond which no bounded steady state exists in response to an increase in the density of defects in the neighbourhood of the surface, using the data in Table I and $W = 1$. The parameter region above the curve corresponds to thermal runaway for all initial conditions.

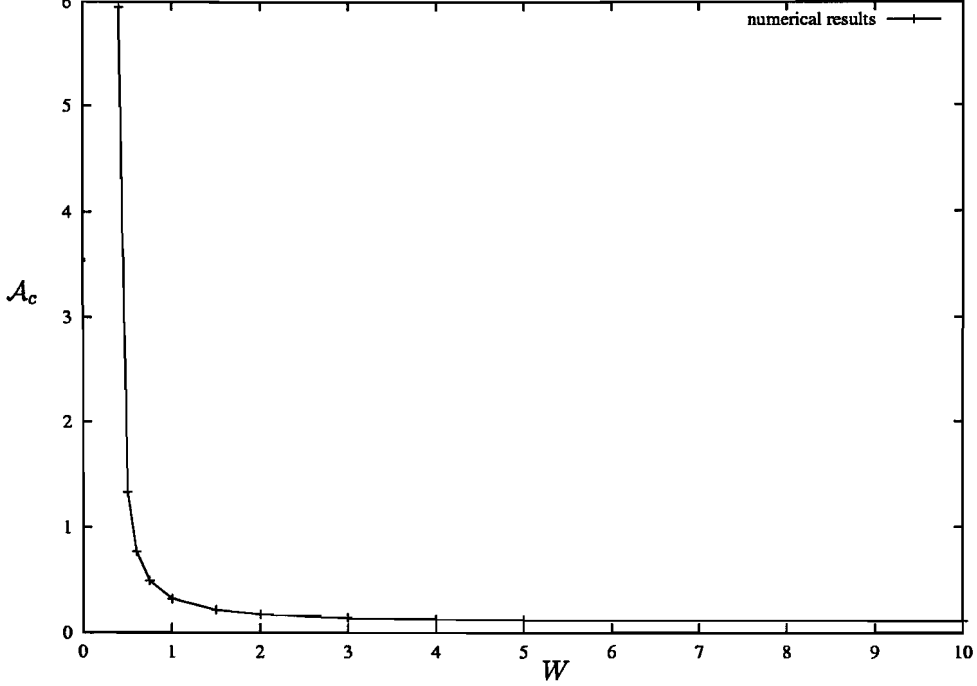

FIG. 4. The decrease in the current beyond which no bounded steady state exists in response to an increase in the length of the region containing a high density of defects, using the data in Table I and $\chi = 4$. The parameter region above the curve corresponds to thermal runaway for all initial conditions.

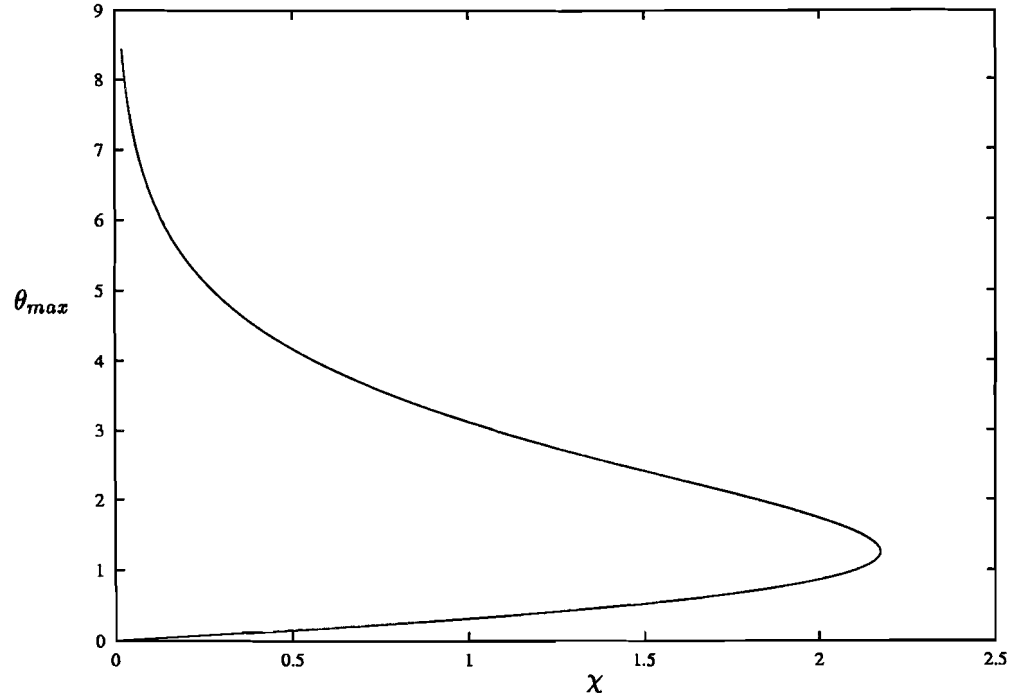

FIG. 5. Typical steady-state response diagram for the maximum temperature θ_{max} plotted against the bifurcation parameter χ. The parameter values are given in Table I except that $\mathcal{A} = 1$, $A_0 = \chi(W - Z_1)$ and $W = 1$.

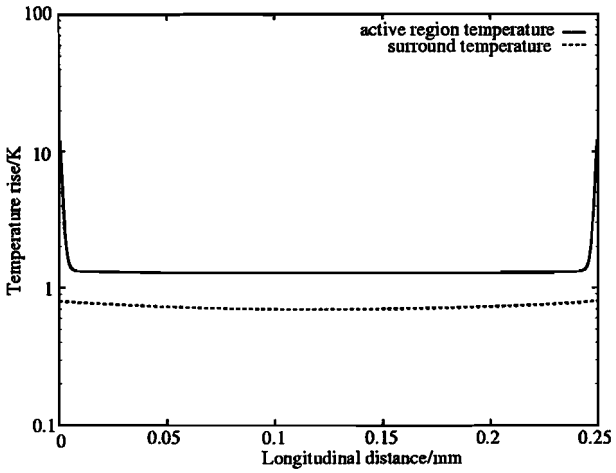

FIG. 6. The numerical solution for the steady-state temperature rise of the active region and surround. The parameter values are given in Table I with $A_0 = 4(W - Z_1)$ and $W = 1$.

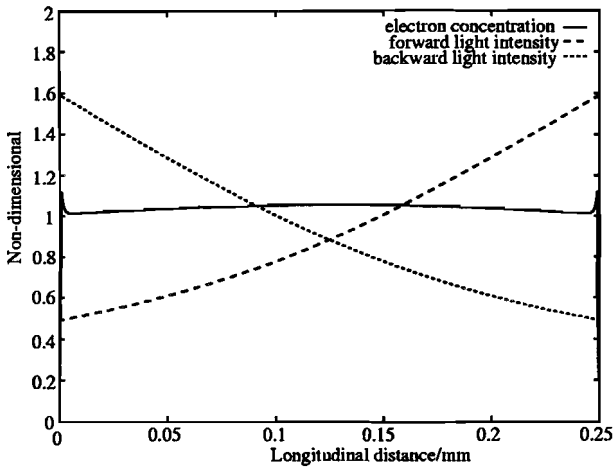

FIG. 7. The numerical solution for the steady-state electron concentration and the light intensities. The parameter values are given in Table I with $A_0 = 4(W - Z_1)$ and $W = 1$, the electron concentration is in units of $1 \times 10^{24} m^{-3}$ and the light intensity is in units of $1 \times 10^{22} m^{-3}$.

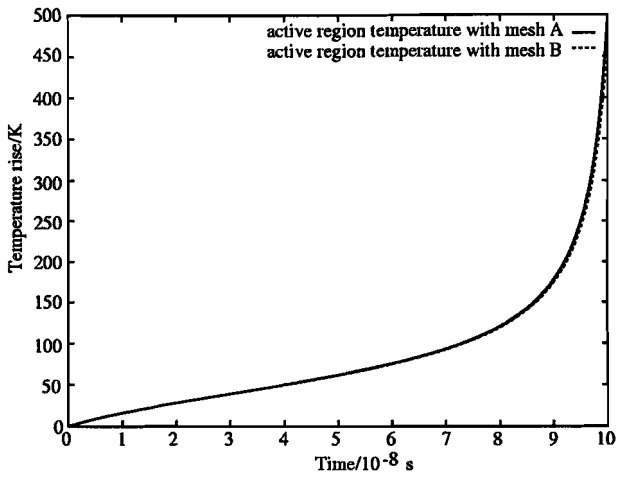

FIG. 8. Numerical solution for the temperature rise of the active region on the mirror facet using two spatial meshes; mesh A being finer than mesh B. The agreement between the two meshes indicates a small relative error. For $A_0 = 4(W - Z_1)$, $W = 1$ and the data used to give Table I except that $\mathcal{A} = 1$ to instigate thermal runaway.

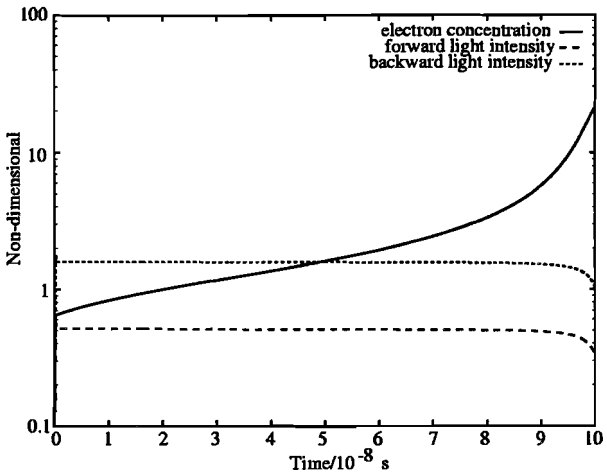

FIG. 9. Numerical solution for electron concentration and the light intensities on the mirror facet. For $A_0 = 4(W - Z_1)$, $W = 1$ and the data used to give Table I except that $\mathcal{A} = 1$ to instigate thermal runaway, the electron concentration is in units of $1 \times 10^{24} m^{-3}$ and the light intensity is in units of $1 \times 10^{22} m^{-3}$.

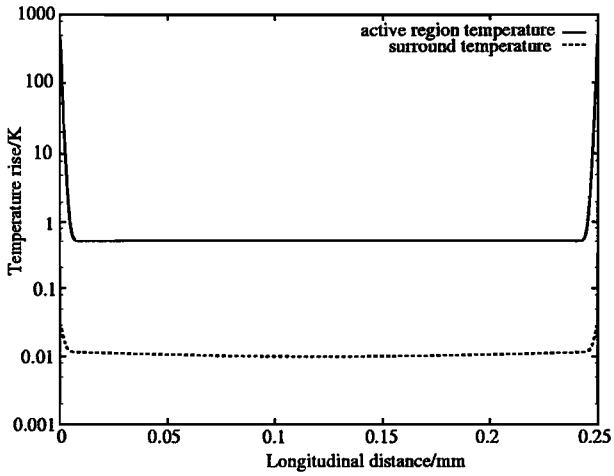

FIG. 10. Numerical solution for the temperature rise of the active region and the surround at $t = 1 \times 10^{-7} s$. For $A_0 = 4(W - Z_1)$, $W = 1$ and the data used to give Table I except that $\mathcal{A} = 1$ to instigate thermal runaway.